

An improved three-band semi-analytical algorithm for estimating chlorophyll-*a* concentration in highly turbid coastal waters: a case study of the Yellow River estuary, China

Jun Chen · Wenting Quan · Zhenhe Wen ·
Tingwei Cui

Received: 7 December 2011 / Accepted: 26 October 2012 / Published online: 20 November 2012
© Springer-Verlag Berlin Heidelberg 2012

Abstract An improved three-band semi-analytical algorithm was developed for improving the performance of the three- and four-band algorithms, for chlorophyll-*a* concentration retrievals in the highly turbid waters of the Yellow River estuary. In this special case study of the Yellow River estuary, the optimal wavelengths of the improved three-band semi-analytical algorithm must meet the following requirements: the λ_1 and λ_2 must be restricted to within the range 660–690 nm, and the λ_3 must be longer than 750 nm. The algorithm calibration and validation results indicate that the improved three-band algorithm indeed produces superior performance in comparison to both the three- and four-band algorithms in retrieving chlorophyll-*a* concentration from the extremely coastal waters of the Yellow River estuary. Comparing the improved three-band algorithm to the original three- and four-band algorithm, the former minimizes the influence of

backscattering by suspended solids in near-infrared regions, while the three-band algorithm has a much stronger error tolerance ability than the four-band algorithm. These findings imply that if an atmospheric correction scheme for visible and near-infrared bands is available, the improved three-band algorithm may be used for quantitative monitoring of chlorophyll-*a* concentration in turbid coastal waters with similar bio-optical properties, although some local bio-optical information or improved models may be required to reposition the optimal band positions of the algorithm.

Keywords Remote sensing · Semi-analytical algorithm · Chlorophyll-*a* concentration · Yellow River estuary

Introduction

According to the optical classification standard given by Morel and Prieur (1977), oceanic waters may be characterized as either Case I, the optical properties of which are dominated by chlorophyll and covarying detrital pigments; or as Case II, in which other substances, which are not only covaried with chlorophyll-*a* (*chl**a*), but are also affected by other optical properties. Such substances include gelbstoff, suspended sediments, coccolithophores, detritus, and bacteria. As a result, pigments retrieved from remote sensing imageries in Case I waters have achieved reasonable results [$\pm 20\%$ for the local best cases (Gordon 1990)], but more research is still required for Case II waters (Moore et al. 2009).

In order to quantify *chl**a* in productive turbid waters, a variety of algorithms have been developed, and all were based on the properties of the reflectance peak near 675 nm (Gitelson 1992), including the ratio of the reflectance peak

J. Chen (✉) · Z. Wen
School of Ocean Sciences, China University of Geosciences,
Beijing 100083, China
e-mail: cjun@cgs.cn

Z. Wen
e-mail: wenzhh@sina.com

J. Chen · Z. Wen
The Key Laboratory of Marine Hydrocarbon Resources and
Environmental Geology, Qingdao Institute of Marine Geology,
Qingdao 266071, China

W. Quan
Shanxi Agriculture Remote Sensing Information Center,
Xian 710000, China

T. Cui
First Institute of Oceanography, State Oceanic Administration,
Qingdao 10083, China

at the NIR (near-infrared) to the reflectance at 670 nm. Gons et al. (2000) used the reflectance ratio at 704 and 672 nm and absorption and backscattering coefficients at these wavelengths to assess chl a concentrations ranging from 3 to 185 mg/m³. Ruddick et al. (2000) analyzed the manner in which errors in reflectance measurements affect chl a retrievals for an NIR to red reflectance ratio algorithm with a general choice of wavelengths. The authors of the said study found that the effects on chl a retrieval depend strongly on the choice of the NIR wavelength if the error is spectrally neutral, suggesting a new type of algorithm, where the NIR wavelength used for retrieval is chosen dynamically for each spectrum to be processed. These approaches rely on a specific spectral feature to biophysical measurements using statistical regression. This type of model is simple and easily implemented (Matthews 2011). However, the method lacks a physical foundation and the relationships within are quite geographically specific and cannot be applied in other areas.

Recently, Dall'Olmo et al. (2003) provided evidence that a three-band reflectance model, originally developed for estimating pigment contents in terrestrial vegetation, could also be used to assess chl a concentration in turbid waters (Gitelson et al. 2008, 2007). This semi-analytical algorithm involved three underlying assumptions (Gitelson et al. 2008; Le et al. 2009): (1) the absorption by suspended solids and CDOM (colored dissolved organic matters) at λ_2 was close to that at λ_1 ; (2) reflectance at λ_3 is minimally affected by the absorption by optically active constituents and could only account for the variability in scattering between samples; and (3) the total backscattering curve is “spectrally flat” in the red and NIR regions. However, the three assumptions for the three-band semi-analytical algorithm may be violated in highly turbid waters, due to the fact that the absorption and scattering of particulate matter at the NIR cannot be ignored in turbid waters (Tassan and Ferrari 2003; Tzitzuiou et al. 2006). Recently, Le et al. (2009) developed a four-band semi-analytical algorithm to improve the performance of the three-band algorithm in turbid waters. The improvement was achieved by subtracting the effects of suspended solids, as well as minimizing the effects of pure water absorption and backscattering in the NIR region using the fourth band. According to the study results carried out by Le et al. (2009), the four-band algorithm showed optimal accuracy in the cases of $\lambda_1 = 663$ nm, $\lambda_2 = 693$ nm, $\lambda_3 = 705$ nm, and $\lambda_4 = 740$ nm. However, the reflectance near 704 nm generally corresponded to the reflectance peak owing to the chl a scattering, whereas the reflectance near 740 nm was indistinctively influenced by the chl a (Gons et al. 2000). As a result, it was difficult for the selected bands of the four-band algorithm to meet the underlying assumption that both $(a_{\text{SSC}} + a_{\text{CDOM}} + a_{\text{chl}a})$ and b_b were spectrally flat in

the red-NIR band (Gitelson et al. 2008). Furthermore, the four-band algorithm used the difference $R_{\text{rs}}^{-1}(\lambda_3) - R_{\text{rs}}^{-1}(\lambda_4)$ as the denominator to eliminate the influence of backscattering by all particulate matter b_b in the numerator. The four-band algorithm suggested that the λ_3 should be quite close to λ_4 in order to meet the requirement of $[a_{\text{chl}a}(\lambda_3) + a_{\text{SSC}}(\lambda_3) + a_{\text{CDOM}}(\lambda_3)] \sim [a_{\text{chl}a}(\lambda_4) + a_{\text{SSC}}(\lambda_4) + a_{\text{CDOM}}(\lambda_4)]$. Thus, the difference $R_{\text{rs}}^{-1}(\lambda_3) - R_{\text{rs}}^{-1}(\lambda_4)$ must be a small value variable, which is many times lower than the difference $R_{\text{rs}}^{-1}(\lambda_1) - R_{\text{rs}}^{-1}(\lambda_2)$. The uncertainty in the numerator, $R_{\text{rs}}^{-1}(\lambda_1) - R_{\text{rs}}^{-1}(\lambda_2)$, would be enlarged if a small number was used as the denominator to divide that numerator (Chen et al. 2010a). As a result, the four-band algorithm may possess poor noise tolerance ability in chl a concentration estimation in turbid waters, which is another limitation of the four-band algorithm.

The main objective of this study is to validate the performance of the three- and four-band algorithms, and to further improve it for use in the Yellow River estuary, China. The specific goals of this study are as follows: (1) to locate the optimal spectral positions of the three- and four-band algorithms; (2) to evaluate the accuracy and stability of the three- and four-band algorithms in predicting chl a in the turbid waters of the Yellow River estuary; (3) to improve the performance of the three-band semi-analytical algorithm by developing an improved semi-analytical algorithm; and (4) to compare the performances of the three- and four-band algorithms with the improved three-band algorithm in terms of estimating chl a concentration in the turbid waters of the Yellow River estuary.

Data, methods and techniques

Study area

The Yellow River estuary is a typical turbid water body, located between 117.58°E and 122.25°E and between 37.10°N and 41.00°N, semi-enclosed by the Bohai Bay and Laizhou Bay of the Bohai Sea, China (Fig. 1). The Yellow River, the second longest river in China, flows into the Yellow River estuary, and is known around the world for its high concentration of sediments. The average run-off is 5.80×10^{10} m³ per year and sediment transport to Bohai Sea is 1.10×10^9 tons per year (Chen et al. 2010b). Consequently, the water column in the Yellow River Estuary is quite turbid, which interferes with the bio-optical properties of the chl a signs and creates a challenge for estimating the chl a concentration from remote sensing data. The Yellow River estuary represents typical turbid coastal waters which are influenced by river and anthropogenic inputs. Chl a concentrations in this area are difficult to estimate accurately as the bio-optical properties of the

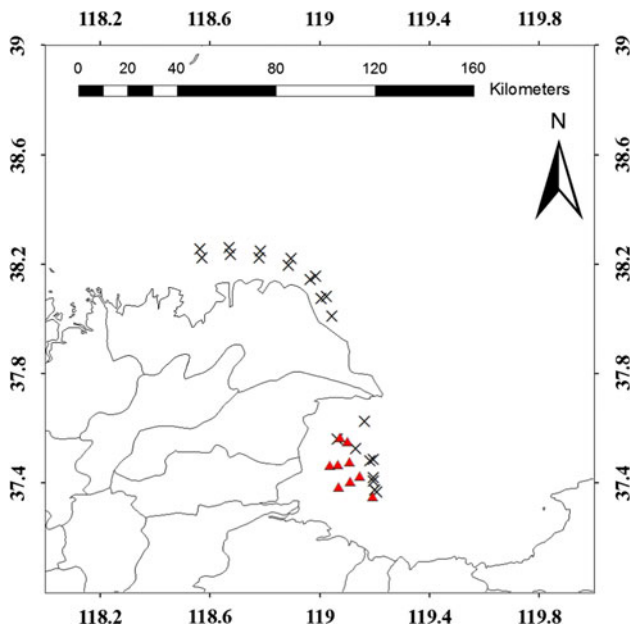


Fig. 1 Yellow River estuary and sample stations.

water bodies are quite complex (Zhang et al. 2010). The signal of the phytoplankton is partially interfered with by the bio-optical properties of SSC and CDOM. As a result, it is challenging to estimate the *chl*_a concentration in the Yellow River estuary due to the high level of SSC. This is the reason why the Yellow River estuary was selected as the study area for use in this paper.

Datasets used

In this study, in order to evaluate the accuracy of the algorithm for estimating *chl*_a concentration, two independent data sets, including the spectral optical properties and *chl*_a concentration of the water column, were collected from the Yellow River estuary. The first data set was used for model calibration, while the second was used for model performance evaluation. The calibration data set containing 24 samples was collected from the Yellow River estuary on 1 and 4 September, 2009. The validation data set containing eight samples was collected from the Yellow River estuary on 10 September, 2009.

Field measurements

The field measurements were conducted from 10:00 to 14:00 local time in the Yellow River estuary. At each station (Fig. 1), water-leaving reflectance measurements were taken from aboard a boat. The reflectance was measured with a spectroradiometer with 25° fiberoptic, covering the spectral range 350–2,500 nm (Spectral Devices, Boulder, CO, ASD). Although data in the range 350–2500 nm, with a spectral resolution of 3 nm (full-

width at half-maximum, FWHM) and a 1.4 nm sampling interval for the 350–1050 nm spectral range (ASD 1999) were collected as well, the data mainly used in this study were those in the range 400–900 nm, which is the most commonly used wavelength for water color remote sensing (Deng and Li 2003; Gons et al. 2008; Ouaidrari and Vermote 1999; Tachiiri 2005; Wang et al. 2009). Following the ocean optics protocols for satellite ocean color sensor validation (Mueller et al. 2003), various measurements were repeated at each station in order to estimate the uncertainty associated with each measurement, and the measurements with <5 % uncertainty were selected for model calibration and validation.

While the measurements were being taken, the tip of the optical fiber was kept ~1 m above the water surface by means of a 3 m long, hand-held black pole. The radiance of both the water surface ($L_{sw}(\lambda)$) and a standard gray board ($L_p(\lambda)$) was measured. Ten curves were acquired for each target. In order to effectively avoid the interference of the ship with the water surface and the influence of direct solar radiation, the instrument was positioned at an angle β of 90–135° with the plane of the incident radiation pointed away from the sun (Le et al. 2009). The view of the water surface, α , was controlled between 30 and 45° with the aplomb direction. In this way, most of the direct sunlight was eliminated while the impact of the ship’s shadow was minimized (Le et al. 2009). Immediately after measuring the water radiance, the spectroradiometer was rotated upwards by 90–120° to measure the skylight. The view azimuth angle in this measurement was kept the same as that when measuring the water radiance (Mueller and Fargion 2002).

Remote sensing reflectance, $R_{rs}(\lambda)$ was calculated as follows:

$$R_{rs}(\lambda) = \frac{L_w(\lambda)}{E_d(0^+, \lambda)} \tag{1}$$

where $L_w(\lambda)$ is the water-leaving radiance, and $E_d(0^+, \lambda)$ is the total incident radiant flux of the water surface. $L_w(\lambda)$ and $E_d(0^+, \lambda)$ in Eq. (1) are further calculated as follows:

$$L_w(\lambda) = L_{sw}(\lambda) - rL_{sky}(\lambda) \tag{2}$$

$$E_d(0^+, \lambda) = \frac{\pi L_p(\lambda)}{\rho_p(\lambda)} \tag{3}$$

where $L_{sky}(\lambda)$ represents the diffused radiation of the sky, which contains no information of water properties and therefore must be eliminated; r refers to the reflectance of the skylight at the air–water interface, the value of which depends upon the solar azimuth, measurement geometry, wind speed, and surface roughness; and $\rho_p(\lambda)$ is the reflectance of the gray plate. In this study, r is calculated with assumption of the black water body at wavelengths from 1,000 to 1,020 nm (Hale and Querry 1973) and

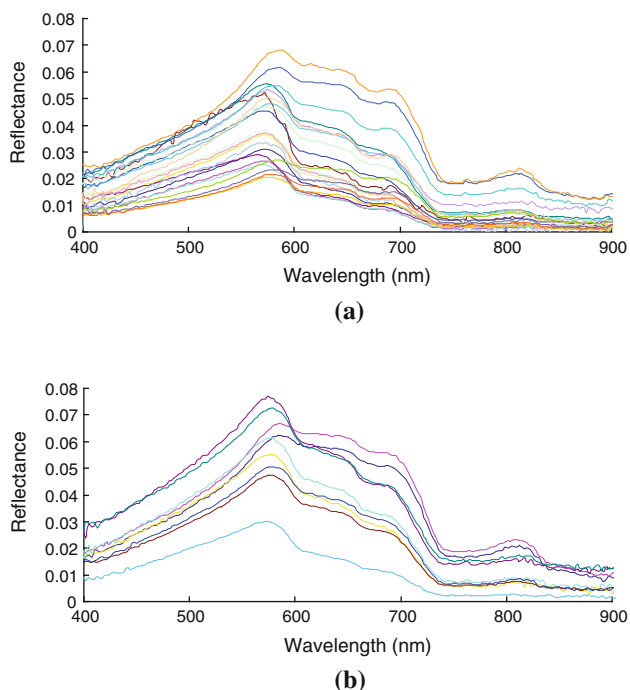


Fig. 2 Field measurement datasets **a** Calibration datasets collected in the Yellow River estuary, China, on 1 and 4 September, 2009. **b** Validation datasets collected in the Yellow River estuary, China, on 10 September, 2009

wavelength-independent (Doxaran et al. 2002). The remote sensing reflectance calculated by Eq. (1) is shown in Fig. 2.

Laboratory measurements

Water samples were collected immediately after the radiance measurements were taken. At each station a standard set of water quality parameters was measured, including *chl a* concentration and transparency. The surface water samples were collected at a depth of 0.5 m below the water–air surface. After sampling, water samples were conserved in bottles at a low temperature and sent for laboratory analysis in the afternoon of the same day.

The laboratory analyses were carried out within 24 h following sample collection. The *chl a* concentrations were extracted and measured with 90 % acetone in accordance with the Ocean Optical Protocols of NASA (Mueller and Fargion 2002), a generally accepted method of quantifying *chl a* concentration in the fields of chemistry and biology (Gilpin and Tett 2001).

Improved semi-analytical algorithm

The $R_{rs}(\lambda)$ model was given according to the following general equation (Morel and Prieur 1977), which was adapted from Lee et al. (1994):

$$R_{rs}(\lambda) = \frac{ft^2}{Q(\lambda)n^2} \frac{b_b(\lambda)}{a(\lambda) + b_b(\lambda)} \quad (4)$$

where f is an empirical factor averaging approximately 0.32–0.33; t is the transmittance of the air–water interface; $Q(\lambda)$ is the upwelling irradiance-to-radiance ratio $E_u(\lambda)/L_u(\lambda)$; and n is the real part of the index of refraction of water. By making the following two approximations, Eq. (4) may be greatly simplified (Carder et al. 2003):

1. In general, f is a function of the solar zenith angle, θ_0 . However, Morel and Gentili (1993) have shown that the ratio f/Q is relatively independent of the θ_0 for sun and satellite viewing angles.
2. t^2/n^2 is approximately equal to 0.54, and although it is capable of changing with sea-state, it is relatively independent of wavelength.

These two approximations lead to a simplified version of Eq. (4):

$$R_{rs}(\lambda) = h \frac{b_b(\lambda)}{a(\lambda) + b_b(\lambda)} \quad (5a)$$

where h is unchanging with respect to λ and θ_0 . The total absorption coefficient may be expanded as follows:

$$a(\lambda) = a_w(\lambda) + a_{chl a}(\lambda) + a_{CDOM}(\lambda) + a_{ssc}(\lambda) \quad (5b)$$

where the subscripts “w”, “chl a”, “CDOM”, and “ssc” refer to water, chl a, CDOM, and suspended sediment, respectively. According to the underlying assumption of three- and four-band algorithms that the $(a_{ssc} + a_{CDOM})$ and b_b are spectrally flat in the red-NIR region, the $R_{rs}^{-1}(\lambda_1) - R_{rs}^{-1}(\lambda_2)$ may be approximated to the following equation:

$$R_{rs}^{-1}(\lambda_1) - R_{rs}^{-1}(\lambda_2) \approx h \frac{a_{chl a}(\lambda_1) + a_w(\lambda_1) - a_w(\lambda_2)}{b_b} \quad (6)$$

Equation (6) is still affected by b_b . If backscattering varies between samples, the model output would be different for the same chl a. To account for this, the $R_{rs}^{-1}(\lambda_3)$ is used in the three-band algorithm, and $R_{rs}^{-1}(\lambda_3) - R_{rs}^{-1}(\lambda_4)$ is used in the four-band algorithm. Hence, the three- and four-band algorithms may be denoted as follows:

$$[chl a] \propto [R_{rs}^{-1}(\lambda_1) - R_{rs}^{-1}(\lambda_2)] R_{rs}(\lambda_3) \quad (7a)$$

$$[chl a] \propto \frac{R_{rs}^{-1}(\lambda_1) - R_{rs}^{-1}(\lambda_2)}{R_{rs}^{-1}(\lambda_3) - R_{rs}^{-1}(\lambda_4)} \quad (7b)$$

where [chl a] is the chl a concentration. The structure of Eq. (5a) originates from Morel and Prieur (1977); when they developed a reflectance model, h was given the mean value of 0.33. As shown in Morel and Gentili (1996), the coefficient h is not constant and does vary in an orderly

manner with the water optical properties. Thus, it is much more challenging to separate $a_{chl a}(\lambda_1)$ from the remote sensing reflectance using the three-band algorithm provided by Gitelson et al. (2008) or the four-band algorithm developed by Lee et al. (2002), due to the poor approximation of Eq. (5a). If considering the water optical properties dependent γ in Eq. (5a), the three- and four-band algorithms should be written as follows:

$$\begin{aligned} & [R_{rs}^{-1}(\lambda_1) - R_{rs}^{-1}(\lambda_2)]R_{rs}(\lambda_3) \\ & \approx \frac{h(\lambda_3) a_{chl a}(\lambda_1) + a_w(\lambda_1) - a_w(\lambda_2)}{h(\lambda_1) a_w(\lambda_3)} \end{aligned} \tag{8a}$$

$$\frac{R_{rs}^{-1}(\lambda_1) - R_{rs}^{-1}(\lambda_2)}{R_{rs}^{-1}(\lambda_3) - R_{rs}^{-1}(\lambda_4)} \approx \frac{h(\lambda_3) a_{chl a}(\lambda_1) + a_w(\lambda_1) - a_w(\lambda_2)}{h(\lambda_1) a_w(\lambda_3) - a_w(\lambda_4)} \tag{8b}$$

Due to the fact that h varies in an orderly manner with the water optical properties, the outputs of the three- and four-band algorithms would be different for the same $chl a$ concentration. To account for this, Gordon et al. (1988) have carried out extensive computations of $R_{rs}(\lambda)$ as a function of the optical properties of the water and solar zenith angle θ_0 , and have concluded that for $\theta_0 \geq 20^\circ$, $R_{rs}(\lambda)$ may be directly related to the inherent optical properties of the water through the following:

$$r_{rs}(\lambda) = \frac{R_{rs}}{0.52 + 1.7R_{rs}} \tag{9a}$$

$$r_{rs}(\lambda) = \frac{s(\lambda)}{s(\lambda) + 1} \left[g_0 + \frac{g_1 s(\lambda)}{s(\lambda) + 1} \right] \tag{9b}$$

$$s(\lambda) = \frac{-g_0 + \sqrt{g_0^2 + 4g_1 r_{rs}(\lambda)}}{2g_1 + g_0 - \sqrt{g_0^2 + 4g_1 r_{rs}(\lambda)}} \tag{9c}$$

where $s(\lambda)$ is the ratio of total backscattering to total absorption; and r_{rs} is remote sensing reflectance spectral measured just below water surface. For nadir-viewed r_{rs} , Gordon et al. (1988) found that $g_0 \approx 0.0949$ and $g_1 \approx 0.0794$ for oceanic Case I waters. Recently, Lee et al. (1999) suggested that $g_0 \approx 0.084$ and $g_1 \approx 0.17$ are more ideal for higher-scattering coastal waters.

The first spectral band must be maximally sensitive to $chl a$. This means that λ_1 must be restricted to within the range 660–690 nm (Gitelson et al. 2008). In order to minimize the influences of absorption by CDOM and suspended sediment at the λ_1 , the second spectral band is used. The second band must meet the requirements of $a_{CDOM}(\lambda_1) \sim a_{CDOM}(\lambda_2)$ and $a_{ssc}(\lambda_1) \sim a_{ssc}(\lambda_2)$. The underlying assumption within is that $a_{CDOM}(\lambda)$ and $a_{ssc}(\lambda)$ are spectrally flat in the red-NIR region (Gitelson et al. 2008). It is worth noting that the improved three-band algorithm does not require λ_2 to be minimum sensitive to absorption by $chl a$, because $[a_{chl a}(\lambda_1) - a_{chl a}(\lambda_2)]$ is still

quite well related to $chl a$ concentration, provided that both $a_{chl a}(\lambda_1)$ and $a_{chl a}(\lambda_2)$ are very well related to $chl a$ concentration. This means that the λ_2 should be set to from 660 to 730 nm, which is beyond the expected wavelength range suggested by Dall’Olmo and Gitelson (2006). The difference $s^{-1}(\lambda_1) - s^{-1}(\lambda_2)$ is still affected by $b_b(\lambda_1)$, i.e. if backscattering varies between samples, the model output would be different for the same $chl a$ concentration. To account for this, a third spectral band, λ_3 , has been adopted. According to the study results carried out by Mobley (1994), Babin and Stramski (2004), and Binding et al. (2008), $a_w > 2.8 \text{ m}^{-1}$ and $a_{ssc} < 0.052 \text{ m}^{-1}$ in highly turbid waters (based on $a_{ssc}(\lambda) = 0.04 \times [\text{SSC}] \times \exp[-0.011(\lambda - 440)]$, where [SSC] refers to SSC concentration), while $\lambda > 750 \text{ nm}$, and SSC concentration is $< 40 \text{ kg/m}^3$. This means that the λ_3 should be set to $> 750 \text{ nm}$ in order to minimize the absorption by suspended sediments in highly turbid waters ($a_w \gg a_{ssc}$). Additionally, in order to minimize the influences of absorption by $chl a$ at the λ_3 in the samples with high $chl a$ concentration (Lee and Carder 2004), the $a_{chl a}(\lambda_3)$ in made non-negligible at the NIR bands in the improved three-band algorithm. Thus, the three-band algorithm may be improved as follows:

$$\begin{aligned} & [s^{-1}(\lambda_1) - s^{-1}(\lambda_2)]s(\lambda_3) \\ & \approx \frac{a_{chl a}(\lambda_1) - a_{chl a}(\lambda_2) + a_w(\lambda_1) - a_w(\lambda_2)}{a_{chl a}(\lambda_3) + a_w(\lambda_3)} \end{aligned} \tag{10}$$

Linear regression of $a_{chl a}(\lambda)$ versus $chl a$ concentration, [chl a], yielded an equation of this form (Carder et al. 2003; Dall’Olmo and Gitelson 2006; Gitelson et al. 2008):

$$a_{chl a}(\lambda) = K_0(\lambda)[chl a] + K_1(\lambda) \tag{11}$$

Substituting Eq. (11) into Eq. (10) and performing simplification then yielded the following improved three-band algorithm:

$$[chl a] = \frac{1}{P_0[s^{-1}(\lambda_1) - s^{-1}(\lambda_2)]s(\lambda_3) + P_1} + P_2 \tag{12}$$

In a similar way, the linear regression of the three- and four-band algorithms may be written as follows:

$$[chl a] = x_0 [R_{rs}^{-1}(\lambda_1) - R_{rs}^{-1}(\lambda_2)]R_{rs}(\lambda_3) + x_1 \tag{13a}$$

$$[chl a] = y_0 \frac{R_{rs}^{-1}(\lambda_1) - R_{rs}^{-1}(\lambda_2)}{R_{rs}^{-1}(\lambda_3) - R_{rs}^{-1}(\lambda_4)} + y_1 \tag{13b}$$

where $x_0, x_1, y_0, y_1, P_0, P_1$, and P_2 are the empirical coefficients determined by the non-linear iterative method suggested by Chen and Quan (2012).

Noise tolerance ability of the $chl a$ estimation algorithm

In this study, the three-band, four-band, and improved three-band algorithms were calibrated and validated

against bio-optical datasets collected from in situ measurements. It may be considered reasonable to ignore the noise of field measurements provided that the bio-optical measurements strictly follow the standards of bio-optical experiments (Mueller and Fargion 2002). However, the final goal of oceanic remote sensing is not only to determine the optimal estimation algorithms from field measurements, but also to accurately estimate the spatial distribution of the *chl a* concentration from satellite images. In fact, the satellite images are contaminated by atmospheric path scattering and absorption, resulting in a residual uncertainty of 5–9 %, even with an accurate atmospheric correction (Chen et al. 2011a; Gordon and Voss 1999; Hu and Carder 2002). Thus, it is necessary to consider the noise tolerance ability of the remote sensing algorithm while applying it to estimating the *chl a* concentration from satellite data.

According to Chen et al. (2010a), the uncertainty caused by a small data noise may be expressed as follows:

$$\Delta[\text{chl}a]_{\text{D}} = \frac{\sum_{i=1}^n \frac{\partial[\text{chl}a]}{\partial R_{\text{rs}}(\lambda_i)} \Delta R_{\text{rs}}(\lambda_i)}{[\text{chl}a]} \quad (14)$$

where $\Delta R_{\text{rs}}(\lambda_i)$ is a data noise at λ_i , $\Delta[\text{chl}a]_{\text{D}}$ is the uncertainty in *chl a* estimation caused by $\Delta R_{\text{rs}}(\lambda_i)$, and n is the number of bands. The principle of Cauchy–Buniakowsky–Schwarz (Chen et al. 2003) suggested that Eq. (14) must meet the following requirement:

$$\Delta[\text{chl}a]_{\text{D}} \leq \frac{\sqrt{2 \sum_{i=1}^n \left(\frac{\partial[\text{chl}a] \Delta R_{\text{rs}}(\lambda_i)}{\partial R_{\text{rs}}(\lambda_i)} \right)^2}}{[\text{chl}a]} \quad (15a)$$

A small noise is generally defined as the ratio of the noise to the measurement value. For the sake of simplicity, in this study it is assumed that the remote sensing reflectance at all bands contains the same residual uncertainty, e.g. the 5 % residual uncertainty in the atmospheric correction of the MODIS and SeaWiFS data obtained during NASA’s mission. This assumption may be unrealistic, but it avoids controversy concerning the exact definition of uncertainty in remote sensing reflectance at each band and its respective method of measurement:

$$\Delta[\text{chl}a]_{\text{D}} \leq k \frac{\sqrt{2 \sum_{i=1}^n \left(\frac{\partial[\text{chl}a]}{\partial R_{\text{rs}}(\lambda_i)} \right)^2 [R_{\text{rs}}(\lambda_i)]^2}}{[\text{chl}a]} \quad (15b)$$

where k , in this study, is defined as a small data noise. In brief, only the case associated with $k = 1 \%$ is discussed here, since any other cases may be linearly denoted using this one. In order to compare different models, noise tolerance ability was normalized by k , denoted as follows:

$$\Delta[\text{chl}a]_{\text{N}} = \frac{\sqrt{2 \sum_{i=1}^n \left(\frac{\partial[\text{chl}a]}{\partial R_{\text{rs}}(\lambda_i)} \right)^2 [R_{\text{rs}}(\lambda_i)]^2}}{[\text{chl}a]} \quad (16)$$

where $\Delta[\text{chl}a]_{\text{N}}$ refers to the normalized $\Delta[\text{chl}a]_{\text{D}}$, that is, the noise tolerance ability defined as the uncertainty in *chl a* estimation caused by 1 % data noise.

Statistical criteria

In order to evaluate algorithm performance, the RMS (root-mean-square) statistic was used in this study. The RMS statistic described here was based on the ratio of root-mean-square error to measured values (O’Reilly et al. 1998). This statistic was described by (Carder et al. 2003):

$$\text{RE} = \left| \frac{[\text{chl}a]_{\text{obs}} - [\text{chl}a]_{\text{mod}}}{[\text{chl}a]_{\text{obs}}} \right| \times 100\% \quad (17a)$$

$$\text{RMS} = \sqrt{\frac{\sum_{i=1}^m \text{RE}_i^2}{m}} \quad (17b)$$

where, $[\text{chl}a]_{\text{mod},i}$ is the modeled value of the i th element, RE is the relative error, RE_i is the relative error of the i th element, $[\text{chl}a]_{\text{obs},i}$ is the observed (or in situ measured) value of the i th element, and m is the number of elements.

Results

Chl a concentration

The data sets used to calibrate and validate the performance of the three-band, four-band, and improved three-band algorithms contained 32 samples of *chl a* concentration. The *chl a* concentration ranged from 1.57 to 13.64 $\mu\text{g/l}$ for the calibration data set, and varied from 2.35 to 6.76 $\mu\text{g/l}$ for the validation dataset (Table 1), indicating that the Yellow River estuary has been slightly eutrophied. The poor correlation (Fig. 3) between *chl a* concentration and transparency emphasizes the fact that *chl a* and the covarying pigment are not the only contributors of water optical properties. Qiao et al. (2009) indicated that the average SSC in the Yellow River estuary may reach as high as $>10 \text{ kg/m}^3$, showing that water of the Yellow River estuary is SSC-rich. Thus, the water of the Yellow River estuary is categorized as extremely turbid Case II.

“Spectrally flat” characteristics at red-NIR regions

According to the results of the study performed by Gitelson et al. (2008), the underlying assumption of the three-band

Table 1 Descriptive statistics of the optical water quality parameters measured: chl a concentration, and transparency (STD refers to standard deviation)

	Min	Max	Median	Average	STD
a. Calibration datasets measured in Yellow River Estuary, China, on 1st and 4th September, 2009, 24 samples					
[chl a], mg/m ³	1.57	13.64	5.68	5.54	5.68
Transparency, 1/m	2.30	0.20	0.90	2.30	0.90
b. Validation datasets measured Yellow River Estuary, China, on 10th September, 2009, 8 samples					
[chl a], mg/m ³	2.35	6.76	5.45	5.15	1.41
Transparency, 1/m	0.30	0.80	0.75	0.65	0.22

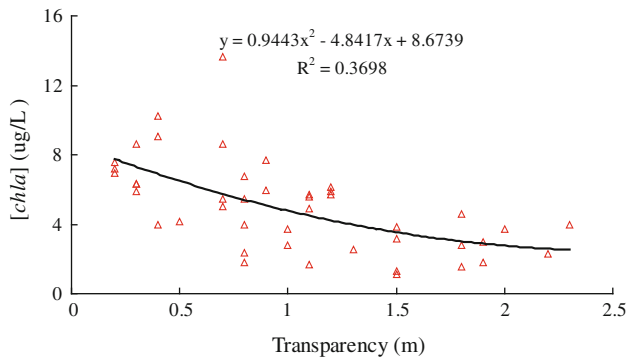


Fig. 3 Chl a concentration plotted against transparency.

algorithm was that $a_{CDOM}(\lambda_1) \sim a_{CDOM}(\lambda_2)$, $a_{SSC}(\lambda_1) \sim a_{SSC}(\lambda_2)$, and $b_b(\lambda_1) \sim b_b(\lambda_2)$ at the red-NIR regions, which also causes the remote sensing reflectance to be “spectrally flat” within those ranges. Thus, the spectral characteristic of the remote sensing reflectance may be used to check the validity of the underlying assumption of the three-band, four-band, and improved three-band algorithms at red-NIR regions. Figure 4 shows the spectral characteristics within the ranges 660–690 nm and 710–730 nm, revealing that the remote sensing reflectance was spectrally flat within the ranges 660–690 nm, but linearly decreased in the range 710–730 nm. Therefore, at least for this data set, the wavelength range 660–690 nm for improved three-band algorithm may be more reasonable than that of 710–730 nm; therefore in this study, the λ_2 of the improved three-band algorithm should be set to the range 660–690 nm.

Algorithm calibration

The optimal positions of the three-band, four-band, and improved three-band algorithms were calculated by the band tuning method, e.g., the λ_1 of the three-band algorithm must be restricted to within the range 660–690 nm; the λ_2 of the three- and four-band algorithms must be restricted to within the range 710–730 nm, while the λ_2 of the improved three-band algorithm must be in the range 660–690 nm; the λ_3 of the three-band algorithm and the λ_3 and λ_4 of the four-band algorithm must be restricted to

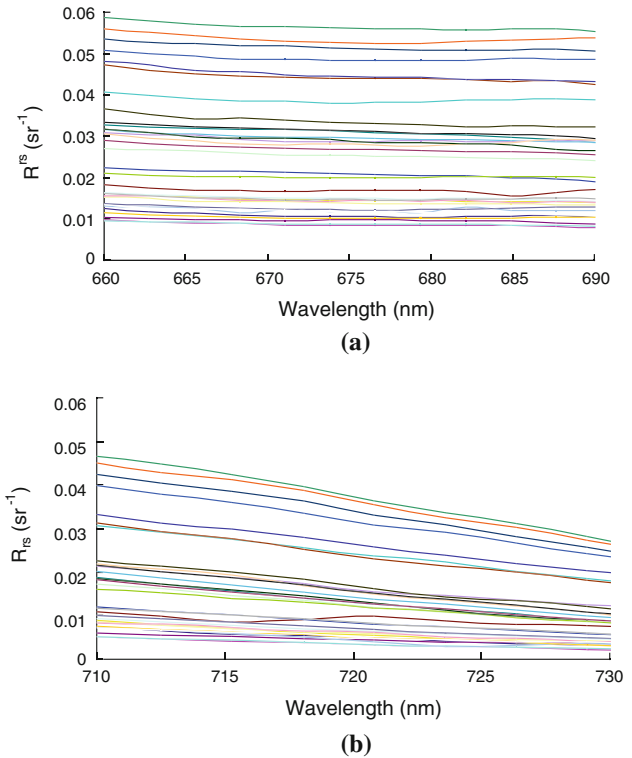


Fig. 4 Spectral characteristics within the ranges 660–690 nm and 710–730 nm, respectively. **a** Spectral characteristics within the range 660–690 nm. **b** Spectral characteristics within the range 710–730 nm

within ranges from the red to NIR wavelengths, while the λ_3 of the improved three-band algorithm must be larger than 750 nm. The non-linear iterative method suggested by Chen and Quan (2012) was used to determine the most ideal functions of the three-band, four-band, and improved three-band algorithms.

Figure 5 showed the optimal three-band, four-band, and improved three-band algorithms, indicating that the three-band algorithm possesses the optimal accuracy in the cases of $\lambda_1 = 668$ nm, $\lambda_2 = 726$ nm, and $\lambda_3 = 765$ nm; the four-band algorithm possesses the optimal accuracy in the cases of $\lambda_1 = 688$ nm, $\lambda_2 = 710$ nm, $\lambda_3 = 671$ nm, and $\lambda_4 = 710$ nm; and the improved three-band algorithm

possesses the optimal accuracy in the cases of $\lambda_1 = 671$ nm, $\lambda_2 = 685$ nm, and $\lambda_3 = 917$ nm. Therefore, the improved three-band algorithm ($R^2 = 0.9168$) produces superior performance in comparison to both the three-band ($R^2 = 0.6963$) and four-band algorithms ($R^2 = 0.8325$).

Algorithm validation

The accuracy and stability in the chl *a* concentration predicted by the three-band, four-band, and improved three-band algorithms were assessed by examining their respective RMS against the validation dataset. Figure 6 shows the accuracy of the three-band, four-band, and improved three-band algorithms assessed by the validation data set, indicating that the improved three-band algorithm produced a superior performance in comparison to both the three- and four-band algorithms, which is consistent with the algorithm calibration results shown in Sect. Algorithm

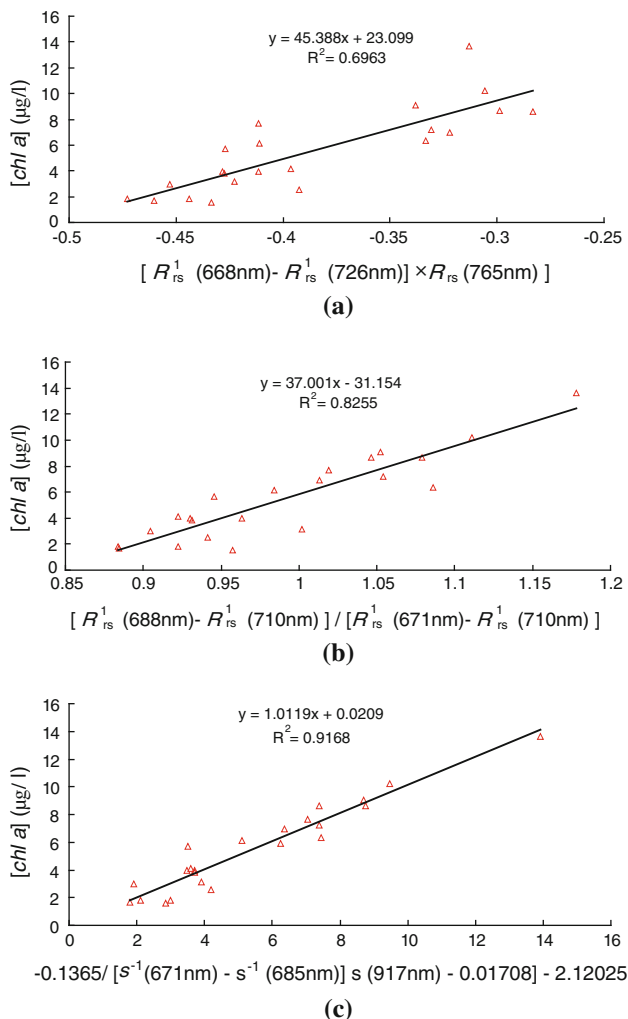


Fig. 5 Optimal **a** three-band, **b** four-band, and **c** improved three-band algorithms in the Yellow River estuary, Chinam

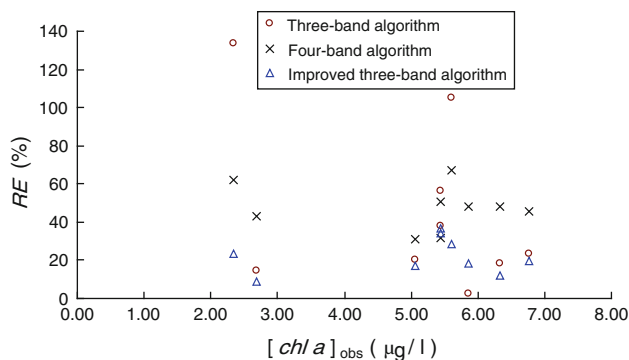


Fig. 6 Performance of three chl *a* estimation algorithm assessed by validation dataset

calibration. Using the improved three-band algorithm in estimating the chl *a* concentration in the Yellow River estuary produced 23.86 % RMS, which decreased 24.93 % RMS from the four-band algorithm and 38.62 % RMS from the three-band algorithm, a significant improvement.

Discussion

Generally speaking, the stability of chl *a* concentration estimation algorithm is greatly dependent on the equivalent degrees of freedom of the chl *a* estimators (Walden 1990), so that although the four-band algorithm produces a superior performance in estimating chl *a* concentration from turbid waters in comparison to the three-band algorithm, its stability may in fact be inferior to the three-band algorithm, due to the fact that the addition of the fourth band also increased the equivalent degrees of freedom of model. In order to illuminate this problem, the calibration data set was used for the noise tolerance ability analysis of these three chl *a* concentration estimation algorithms. Figure 7 shows the noise tolerance ability of three-band, four-band, and improved band algorithms computed by Eq. (16), indicating that the improved three-band algorithm possesses a superior noise tolerance ability in comparison to both the three- and four-band algorithms. It is generally considered reasonable to ignore the residual uncertainty of field measurements provided that the bio-optical measurements strictly follow the standards of bio-optical experiments (Mueller and Fargion 2002). However, the final goal of oceanic remote sensing is not only to construct optimal estimation algorithms from field measurements, but also to accurately estimate the chl *a* concentration from satellite images. Noise tolerance ability is of importance to algorithms for estimating chl *a* concentration in turbid waters from satellite data. The results of this study suggest that an optimal algorithm should not only have a good chl *a* concentration prediction ability, but it should also have an excellent noise tolerance ability for noise of remote sensing

imagery. Accordingly, from the perspectives of both noise tolerance ability and chl_a prediction ability, the improved three-band algorithm is the most ideal of the three algorithms.

Due to the poor approximation of Eq. (4) developed by Morel and Prieur (1977), the absorption by chl_a cannot be very well isolated by either the three- or four-band algorithms. A more accurate remote sensing reflectance model developed by Gordon et al. (1988) is used to construct the improved three-band algorithm. Moreover, compared to the three-band algorithm, the improved three-band algorithm removes the backscattering of suspended solids over the NIR region more effectively, and when compared to the four-band algorithm, the improved three-band algorithm is more capable of reducing the equivalent degrees of freedom. The calibration and validation results indicate that all three of the algorithms produce good performance in terms of estimating chl_a concentration in the Yellow River estuary, but the improved three-band algorithm provides a performance which is superior to both the three- and four-band algorithm, not only in terms of chl_a prediction ability, but also in terms of noise tolerance ability.

The improved three-band algorithm presented in this study may be applied to NASA HYPERION and the Compact High Resolution Imaging Spectrometer (CHRIS). As an example, the HYPERION channels at 681 nm and 915 nm is closed to the position of $\lambda_2 = 685$ and $\lambda_3 = 917$ nm, respectively, and the 32nd channel of HYPERION is located at the position of $\lambda_1 = 671$ nm. A comparison of the measured and predicted estimates of the chl_a by using the improved three-band algorithm with HYPERION spectral bands is presented in Fig. 8, and the results indicate that the improved three-band algorithm with HYPERION spectral bands produces good performance in estimating the chl_a concentration in the Yellow River estuary, the regression coefficient of which is 0.8997, and the corresponding RMS is 27.23 %. These findings imply that, provided that an atmospheric correction scheme for visible and near-infrared bands is available, the

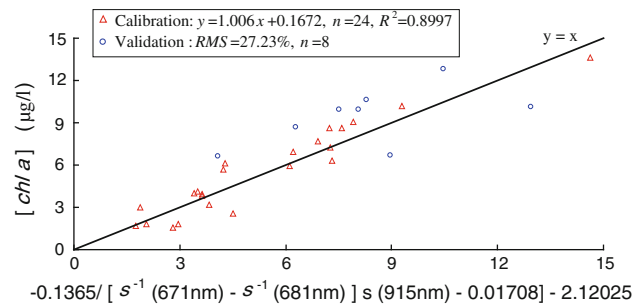


Fig. 8 Chl_a concentrations measured in Yellow River estuary reservoirs in October, 2009 plotted versus chl_a concentration predicted by the improved three-band algorithm using HYPERION spectral bands

improved three-band algorithm may be used for the quantitative monitoring of chlorophyll-*a* concentration from the HYPERION sensor in the Yellow River estuary.

One limitation of this study is that the calibration and validation datasets contained only a narrow range of optical properties of natural turbid waters, being collected only from the Yellow River estuary. The results are insufficient to completely validate the accuracy of the algorithms in other waters with different bio-optical properties. Thus, it is concluded that the improved algorithm should be used for estimating chl_a in highly turbid coastal waters, although it may be necessary to accordingly reposition the wavelengths of the three bands for the given aquatic bio-optical conditions. The researchers also suggest calibration and validation of the algorithms based on more in situ measurements of waters with different optical properties.

Summary

In this study, an improved three-band algorithm was developed and constructed. The results suggest that the optimal wavelengths of the improved three-band semi-analytical algorithm must meet the requirements of the λ_1 and λ_2 being restricted to within the range 660–690 nm, and the λ_3 must be longer than 750 nm. The respective performances of the three-band, four-band, and improved three-band algorithms were validated and assessed using bio-optical datasets collected from the turbid waters of the Yellow River estuary, China. By comparison, using the improved three-band algorithm in estimating chl_a concentration from the Yellow River estuary, uncertainty decreased by 24.93 % compared to the four-band algorithm, and 38.62 % compared to the three-band algorithm. The noise tolerance ability is of importance to algorithms for estimating chl_a concentration in turbid waters. The researchers advise that an optimal algorithm must not only have a good chl_a concentration prediction ability, but it must also possess an excellent noise tolerance ability in

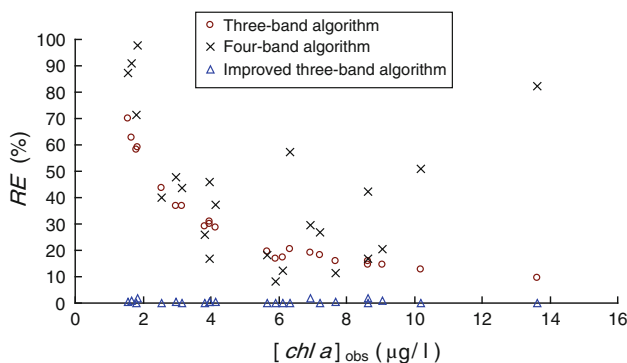


Fig. 7 Anti-disturbance ability of three-band algorithm, four-band algorithm and improved three-band algorithm

order to decrease the impacts of residual data uncertainty of satellite imagery when performing the *chl_a* concentration estimation. Due to its good performance in noise tolerance ability and *chl_a* concentration estimation accuracy, the improved three-band algorithm is superior to both the three- and four-band algorithms, and may be used for retrieving chlorophyll-*a* concentration from extremely turbid waters with similar bio-optical properties, although it may be necessary to reposition the optimal band positions of the algorithm using local bio-optical information.

Acknowledgments This study is supported by the Science Foundation for 100 Excellent Youth Geological Scholars of China Geological Survey, open fund of Key Laboratory of Marine Hydrocarbon Resources and Environmental Geology (MRE201109), High-tech Research and Development Program of China (No. 2007AA092102), and Dragon 3 Project (ID 10470). We would like to just express our gratitude to two anonymous reviewers for their useful comments and suggestions.

References

- ASD (1999). Analytic Spectral Devices. Inc. Technical Guide, 3rd Ed
- Babin M, Stramski D (2004) Variations in the mass-specific absorption coefficient of mineral particles suspended in water. *Limnol Oceanogr* 49(3):756–767
- Binding CE, Jerome JH, Bukata RP, Booty WG (2008) Spectral absorption properties of dissolved and particulate matter in Lake Erie. *Remote Sens Environ* 112:1702–1711
- Carder KL, Chen FR, Lee ZP, Hawes SK, Cannizzaro JP (2003) MODIS Ocean Science Team Algorithm Theoretical Basis Document: Case 2 chlorophyll *a*. ATBD 19, Version 7
- Chen J, Quan WT (2012) An improved algorithm for retrieving chlorophyll-*a* from the Yellow River Estuary using MODIS imagery. *Environ Monit Assess*. doi:10.1007/s10661-10012-12705-y
- Chen JX, Yu CH, Jin L (2003) Mathematical analysis, 4th edn. Higher Education Press, Beijing
- Chen J, Zhou GH, Wen JG, Fu J (2010a) Effect of remotely sensed data errors on the retrieving accuracy of territorial parameters. *Spectrosc Spectr Anal* 30(5):1347–1350
- Chen XL, Lu JZ, Cui TW, Jiang WS, Tian LQ, Chen LQ, Zhao WJ (2010b) Coupling remote sensing retrieval with numerical simulation for SPM study-Taking Bohai Sea in China as a case. *Int J Appl Earth Obs Geoinf* 12S:S203–S211
- Chen J, Fu J, Zhang MW (2011a) An atmospheric correction algorithm for Landsat/TM imagery basing on inverse distance spatial interpolation algorithm: a case study in Taihu Lake. *J Sel Appl Earth Observ Remote Sens*. doi:10.1109/JSTARS.2011.2150200
- Chen J, Wen ZH, Fu J, Sun JH, Wang BJ, Gao XJ (2011b) The application and principle of water quality remote sensing, vol 1. Ocean Press, Beijing
- Dall’Olmo G, Gitelson AA (2006) Effect of bio-optical parameter variability and uncertainties in reflectance measurements on the remote estimation of chlorophyll-*a* concentration in turbid productive waters: modeling results. *Appl Opt* 45(15):3577–3592
- Dall’Olmo G, Gitelson AA, Rundquist DC (2003) Towards a unified approach for remote estimation of chlorophyll-*a* in both terrestrial vegetation and turbid productive water. *Geophys Res Lett* 30. doi:10.1029/2003GL0108065
- Deng M, Li Y (2003) Use of SeaWiFS imagery to detect three-dimensional distribution of suspended sediment. *Int J Remote Sens* 24(3):519–534
- Doxaran D, Froidefond JM, Lavender S, Castaing P (2002) Spectral signature of highly turbid water application with SPOT data to quantify suspended particulate matter concentration. *Remote Sens Environ* 81(1):149–161
- Gilpin L, Tett P (2001) A methods for analysis of benthic chlorophyll-*a* pigment. In: Marine biology report. Napier University Press, UK, pp 326–341
- Gitelson AA (1992) The peak near 700 nm on reflectance spectra of algae and water: relationships of its magnitude and position with chlorophyll concentration. *Int J Remote Sens* 13:3367–3373
- Gitelson AA, Schalles JF, Hladik CM (2007) Remote chlorophyll-*a* retrieval in turbid, productive estuaries: Chesapeake Bay case study. *Remote Sens Environ* 109:464–472
- Gitelson AA, Dall’Olmo G, Moses W, Rundquist DC, Barrow T, Fisher TR, Gurlin D, Holz J (2008) A simple semi-analytical model for remote estimation of chlorophyll-*a* in turbid waters: validation. *Remote Sens Environ* 112:3582–3593
- Gons HJ, Rijkeboer M, Bagheri S, Ruddick KG (2000) Optical Teledetection of chlorophyll *a* in Estuarine and Coastal Waters. *Environ Sci Technol* 34:5189–5192
- Gons HJ, Auer MT, Effler SW (2008) MERIS satellite chlorophyll mapping of oligotrophic and eutrophic waters in the Laurentian Great Lakes. *Remote Sens Environ* 112:4098–4106
- Gordon HR (1990) Radiometric considerations for ocean color remote sensing. *Appl Opt* 29:3228–3236
- Gordon HR, Voss KJ (1999) MODIS normalized water-leaving radiance algorithm theoretical basis document. NASA Technic Document, Under Contract Number NAS5-31363, Version 31364
- Gordon HR, Brown OB, Evans RH, Brown JW, Smith RC, Baker KS, Clark DK (1988) A semianalytic radiance model of ocean color. *J Geophys Res* 93:10909–10924
- Hale GM, Querry MR (1973) Optical constants of water in the 200 nm to 200 micrometer meter wavelength region. *Appl Opt* 12(3):555–563
- Hu CM, Carder KL (2002) Atmospheric correction for airborne sensors: comment on a scheme used for CASI. *Remote Sens Environ* 79:134–137
- Le CF, Li YM, Zha Y, Sun DY, Huang CC, Lu H (2009) A four-band semi-analytical model for estimating chlorophyll *a* in highly turbid lakes: the case of Taihu Lake, China. *Remote Sens Environ* 113:1175–1182
- Lee ZP, Carder KL (2004) Absorption spectrum of phytoplankton pigments derived from hyperspectral remote-sensing reflectance. *Remote Sens Environ* 89(3):361–368
- Lee ZP, Carder KL, Hawes SH, Steward RG, Peacock TG, Davis CO (1994) A model for interpretation of hyperspectral remote sensing reflectance. *Appl Opt* 33:5721–5732
- Lee ZP, Carder KL, Mobley CD, Steward RG, Patch JS (1999) Hyperspectral remote sensing for shallow waters. 2. Deriving bottom depths and water properties by optimization. *Appl Opt* 38:3831–3843
- Lee ZP, Carder KL, Arnone RA (2002) Deriving inherent optical properties from water color: a multiband quasi-analytical algorithm for optically deep waters. *Appl Opt* 41(27):5755–5772
- Matthews MW (2011) A current review of empirical procedures of remote sensing in inland and near-coastal transitional waters. *Int J Remote Sens* 32(21):6855–6899
- Mobley CD (1994) Light and water: radiative transfer in natural waters. Academic Press, New York
- Moore TS, Campbell JW, Dowell MD (2009) A class-based approach to characterizing and mapping the uncertainty of the MODIS ocean chlorophyll product. *Remote Sens Environ* 113:2424–2430

- Morel A, Gentili B (1993) Diffuse reflectance of oceanic waters, II. Bi-directional aspects. *Appl Optical* 30:4427–4438
- Morel A, Gentili B (1996) Diffuse reflectance of oceanic waters. III. Implication of bidirectionality for the remote sensing problem. *Appl Opt* 35(24):4850–4613
- Morel A, Prieur L (1977) Analysis of variances in ocean color. *Limnol Oceanogr* 22:709–722
- Mueller JL, Fargion GS (2002). Ocean optics protocols for satellite ocean color sensor validation. SeaWiFS Technical Report Series, Revision 3 Part II, pp 171–179
- Mueller JL, Davis CO, Arnone RA, Frouin R, Carder KL, Lee ZP, Steward RG, Hooker S, Mobley CD, McClain CR (2003) Above-water radiance and remote sensing measurement and analysis protocols. Ocean Optics Protocols for Satellite Ocean-Color Sensor Validation, Revision 4, Vol. III: Radiometric Measurements and Data Analysis Protocols, NASA Tech. Memo, pp 2003–21162
- O'Reilly JE, Maritorena S, Mitchell BG, Siegel DA, Carder KL, Garver SA, Kahru M, McClain C (1998) Ocean color chlorophyll algorithms for SeaWiFS. *J Geophys Res* 103(11):937–953
- Ouadrari H, Vermote EF (1999) Operational atmospheric correction of Landsat TM data. *Remote Sens Environ* 70:4–15
- Qiao SQ, Shi XF, Zhu AM, Liu YG, Bi NS, Fang XS, Yang G (2009) Distribution and transport of suspended sediments off the Yellow River mouth and the nearby Bohai Sea. *Estuar Coast Shelf Sci*. doi:10.1016/j.ecss.2009.1007.1019
- Ruddick KG, Ovidio F, Rijkeboer M (2000) Atmospheric correction of SeaWiFS imagery for turbid coastal and inland waters. *Appl Opt* 39:897–912
- Tachiiri K (2005) Calculating NDVI for NOAA/AVHRR data after atmospheric correction for extensive images using 6S code: a case study in the Marsabit District, Kenya. *ISPRS J Photogrammetry Remote Sensing* 59:103–114
- Tassan S, Ferrari GM (2003) Variability of light absorption by aquatic particles in the near-infrared spectral region. *Appl Opt* 42:4802–4810
- Tzitzuiou M, Herman JR, Gallegos CL, Neale PJ, Subramanian A, Harding LW, Ahmad Z (2006) Determination of chlorophyll content and trophic state of lakes using field spectrometer and IRS-IC satellite data in the Mecklenburg Lake District, Germany. *Remote Sens Environ* 73:227–235
- Walden AT (1990) Variance and degrees of freedom of a spectral estimator following data tapering and spectral smoothing. *Signal Process* 20:67–79
- Wang MH, Son SH, Shi W (2009) Evaluation of MODIS SWIR and NIR-SWIR atmospheric correction algorithms using SeaBASS data. *Remote Sens Environ* 113:635–644
- Zhang MW, Tang JW, Dong Q, Song QT, D J (2010) Retrieval of total suspended matter concentration in the Yellow and East China Seas from MODIS imagery. *Remote Sens Environ* 114:392–403